INTERNATIONAL JOURNAL FOR NUMERICAL METHODS IN FLUIDS
Int. J. Numer. Meth. Fluids 2009; **61**:255–274
Published online 11 November 2008 in Wiley InterScience (www.interscience.wiley.com). DOI: 10.1002/fld.1955

Method of fundamental solutions for partial-slip fibrous filtration flows

Shunliu Zhao and Alex Povitsky*, †

Department of Mechanical Engineering, The University of Akron, Akron, OH 44325-3903, U.S.A.

SUMMARY

In this study a Stokeslet-based method of fundamental solutions (MFS) for two-dimensional low Reynolds number partial-slip flows has been developed. First, the flow past an infinitely long cylinder is selected as a benchmark. The numerical accuracy is investigated in terms of the location and the number of the Stokeslets. The benchmark study shows that the numerical accuracy increases when the Stokeslets are submerged deeper beneath the cylinder surface, as long as the formed linear system remains numerically solvable. The maximum submergence depth increases with the decrease in the number of Stokeslets. As a result, the numerical accuracy does not deteriorate with the dramatic decrease in the number of Stokeslets. A relatively small number of Stokeslets with a substantial submergence depth is thus chosen for modeling fibrous filtration flows. The developed methodology is further examined by application to Taylor–Couette flows. A good agreement between the numerical and analytical results is observed for no-slip and partial-slip boundary conditions. Next, the flow about a representative set of infinitely long cylindrical fibers confined between two planar walls is considered to represent the fibrous filter flow. The obtained flowfield and pressure drop agree very well with the experimental data for this setup of fibers. The developed MFS with submerged Stokeslets is then applied to partial-slip flows about fibers to investigate the slip effect at fiber–fluid interface on the pressure drop. The numerical results compare qualitatively with the analytical solution available for the limit case of infinite number of fibers. Copyright © 2008 John Wiley & Sons, Ltd.

Received 14 January 2008; Revised 30 August 2008; Accepted 23 September 2008

KEY WORDS: method of fundamental solutions; micro-fluids; partial-slip boundary conditions; Stokeslets; fibrous filtration; Stokes flow

1. INTRODUCTION

In the filtration process, particles are separated from the fluid mainly by interception, inertial impaction and Brownian diffusion [1–3] toward fibers. The flowfield about fibers and the pressure

*Correspondence to: Alex Povitsky, Department of Mechanical Engineering, The University of Akron, Akron, OH 44325-3903, U.S.A.
†E-mail: povitsky@uakron.edu

drop across the setup of fibers are important to predict the filter efficiency. In frame of the Stokes approximation ($Re<1$), Kuwabara and Hapel independently proposed two similar sets of analytical solutions to the fibrous filtration flow, which was represented by a two-dimensional flow past a cylindrical fiber with symmetrical boundary conditions (BC) [4, 5]. Based on the simple Kuwabara's and Hapel's model, also called the cell model, there have been a number of numerical studies about the flowfield, pressure drop and particle capture mechanisms [6–9]. As shown in [10], Kuwabara's model is applicable to strictly periodically arranged fibers.

Most of the prior studies are concerned with the no-slip flows ($Kn\leqslant 0.01$), where Kn is the Knudsen number [1, 11]. If $0.01<Kn\leqslant 0.25$, velocity slip at the fiber surface needs to be accounted for due to the presence of Knudsen layer at the fiber wall [1]. Again, analytical solutions based on the cell Kuwabara's model have been proposed for filtration flows in the partial-slip flow regime [1, 10]. It was shown that the filter efficiency increases with the increase in the Knudsen number in the slip flow regime [12].

Modeling of flowfield to predict particles' dynamics and material adsorption in fibrous structures is of significant interest. Although cell models for predicting the capture efficiency and pressure drop of fibrous media are available [6–9, 13], more detailed models of flowfield are currently needed, for example, to predict the position of the adsorbed particles within the multi-modal non-structured fiber web [14]. An adequate model of flowfield is important to understand fouling and caking that can render the filter ineffective [15]. For signaling and sensing [16], it is crucial to monitor and predict positions of the captured particles, for which purpose the flowfield model is needed.

Filters made of nanofibers are important to capture nano-scale particles since usually the size of the capturing particles is comparable to the size of the fibers. For gas flows in filters, partial-slip BC are valid if the Knudsen number, defined as the ratio of the mean free path over a characteristic length [1, 11], satisfies $0.01<Kn<0.25$. The mean free path in air under standard conditions is $\sim$ 72 nm so the flowfield about fibers ranging from 0.25 to 7 μm of radius will have partial-slip BC. For liquid flows in filters, apparent slip [17], ranging from nanometers [18] to micrometers [19], has been reported in the literature. Thus, partial-slip BC are important for gas and liquid filtration flows.

Numerical techniques for solving Stokes equations can be categorized into either domain-discretization method such as finite-volume methods, or boundary-discretization method such as the method of fundamental solutions (MFS). The boundary-discretization methods are more feasible for complex geometry of multiple fibers compared with the domain-discretization methods. The boundary-discretization methods may become particularly important for dynamically changing geometry of the setup because of flow pressure exerted on fibers and formation of clouds of captured particles at the fibers' surface. The boundary-discretization methods usually have a lower storage and computational time requirements than the domain-discretization methods. However, the practical use of the MFS is hindered by the presence of singularities and other problems related to the ill-conditioned matrix associated with the MFS [20, 21].

The goal of this paper is twofold: (1) to extend the MFS to two-dimensional partial-slip Stokes flows and to minimize the required number of boundary elements by the systematic choice of their location; and (2) to apply the developed methodology to fibrous filtration flows with the finite number of fibers.

This study is aimed at developing a robust numerical method suitable for filtration flows for the finite number of fibers in the no-slip and partial-slip flow regimes. Filtration flows for finite multi-fiber setup have been studied numerically and compared with available experiments. In general,

DOI: 10.1002/fld

the number of fibers required to represent the filter depends on the level of irregularity of fibers' web. The finite-difference [22] and spectral domain-based methods [23] have been used to simulate the filtration flows through cylindrical fibers. The variational and boundary element methods have been applied to study filtration flows through elliptical fibers [1]. A boundary collocation method was employed to model filtration flows through porous cylindrical fibers [24].

Two-dimensional Stokes flows have been extensively studied theoretically, experimentally and numerically. Consequently, a number of equivalent forms of the Stokes equations were proposed in terms of vorticity, pressure and stream function, such as the harmonic equations of vorticity and pressure and bi-harmonic equations of stream function [25]. The vorticity and stream function-based methods are limited to two-dimensional flows, whereas the considered MFS method can be extended to three-dimensional flows. Such an extension is important for bended and randomly oriented fibers, fibers of finite length and to the problem of interception of spherical particles by fibers. Our recent papers [26, 27] extended MFS to motion (assembly) of three-dimensional isolated particles in still fluid for setups for up to four spherical particles; however, fibrous flows were out of scope of those papers.

As one of the boundary-discretization-based methods, the MFS has been successfully applied to a number of two- and three-dimensional steady Stokes flows, such as cavity flows [21], cavity flows with cylinders [28], flows caused by the motion of solid particles [29, 30], flows about two spheres in tandem [31], spiral swimming flows [32, 33], and movement of spherical particles in capillaries [34], to name a few. Efforts also have been made to solve unsteady Stokes flows by the singularity method [25, 35, 36] and inverse two-dimensional Stokes problems [37]. The MFS has also been applied to Brinkman flow including the case of Brinkman flow with Robin BC at the interface with another fluid [38]. In these applications, the flows assumed to have no-slip BC at rigid boundaries. Attempts were made to define the optimal location of the singularities [29, 39–42]; however, systematic study is still needed to find the minimum number of singularities to solve the Stokes flow with the required accuracy. The needed number of singularities appears to be a function of the submergence depth of singular points. In particular, such an investigation is needed for setups with the finite, but considerable number of fibers for which an unreasonable large number of boundary singularities may be required otherwise.

In the MFS, the solution is formed by superposing the fundamental solutions to the Stokes equations. The strength of the singularities is then obtained by solving a system of linear equations formed by enforcing the solution to satisfy the BC by direct collocation or by a least-squares fitting [43]. The Stokeslet, the primary singularity of the Stokes equations [44], and the direct collocation procedure are adopted in this study. In this study, the flow past an infinite long cylinder was selected as a benchmark. The numerical accuracy is investigated thoroughly as functions of location and the number of Stokeslets. It is shown that the number of Stokeslets can be dramatically reduced to achieve a prescribed accuracy by optimizing the location of Stokeslets.

The developed methodology was then applied to investigate the no-slip and partial-slip flows about representative sets of cylinders confined between two planar walls. The effect of setup parameters on the pressure drop was examined. The obtained velocity profiles and pressure drop across the filter compare favorably with the results of an experiments performed recently for no-slip flow about the finite number of fibers [45]. The slip effect is then investigated over the velocity profile and the pressure drop. The influence of the number of rows and columns of fibers on the pressure drop is investigated. Although the physical model of the finite setup of fibers considered in this study is different from Kuwabara's cell model, it is shown that the numerical pressure drop approaches Kuwabara's solution when the number of rows of fibers increases.

DOI: 10.1002/fld

The paper is composed as follows. In Section 2, the mathematical model is presented and the solution method based on the MFS is described. In this section, the differentiation of Stokeslets is introduced to match the partial-slip BC. In Section 3, the proposed MFS for partial-slip flows is validated against two benchmark circular geometry flows: (i) the flow past an infinitely long cylinder and (ii) the flow confined in the gap between two concentric rotating cylinders. In Section 4, the developed MFS is implemented to filtration flows. The obtained numerical results agree well with the experimental data available for the no-slip filtration flow. For flow with partial-slip BC in the same fibrous system, the numerical results are compared with the analytical Kuwabara's model. In Section 5, the conclusions are drawn and future work is discussed briefly.

2. MATHEMATICAL MODEL AND SOLUTION METHOD

2.1. Governing equations and boundary conditions

The governing equations are the Stokes equations. The associated partial-slip and no-penetrating BC in the polar coordinate system are

$$\begin{aligned} u_\theta &= u_{s\theta} + c\left(\frac{1}{r}\frac{\partial u_r}{\partial \theta} - \frac{1}{r}u_\theta + \frac{\partial u_\theta}{\partial r}\right)_{r=a} \\ u_r &= u_{sr} \end{aligned} \tag{1}$$

where $c=((2-\sigma)/\sigma)Kn\,a$ is the coefficient of partial-slip BC, Kn is the Knudsen number, a is the radius of cylinder, σ is the tangential momentum accommodation coefficient, $u_{s\theta}$ and u_{sr} are the θ and r components of the wall velocity. When $Kn=0$, $c=0$ and the partial-slip BC reduce to the no-slip BC.

2.2. MFS with two-dimensional Stokeslets

The primary singularity, Stokeslet, was used in the method of fundamental solutions in the current study. The velocity induced by a Stokeslet, or point force, is given by [25]

$$u^{(k)} = \frac{1}{4\pi\mu}\left(F^{(k)} \ln|\vec{r}| - \frac{F^{(m)} r^{(m)}}{|\vec{r}|^2} r^{(k)}\right) \tag{2}$$

where $\vec{F}(F^{(1)}, F^{(2)})$ is the Stokeslet composed of scalar components $F^{(1)}$ and $F^{(2)}$, μ is the viscosity, $\vec{r}$ is the vector directed from the observation point (also referred to as collocation point) to the Stokeslet (see Figure 1(b)), $|\vec{r}|$ is the magnitude of vector $\vec{r}$, the superscripts k and m denote the components of vectors. The Einstein summation rule applies to the superscript m.

Because of the linearity of the Stokes equations, the velocity induced by N Stokeslets is the summation of fundamental solutions,

$$u_j^{(k)} = \frac{1}{4\pi\mu}\sum_{i=1}^{N}\left(F_i^{(k)} \ln|\vec{r}_{ij}| - \frac{F_i^{(m)} r_{ij}^{(m)}}{|\vec{r}_{ij}|^2} r_{ij}^{(k)}\right) \tag{3}$$

where $\vec{r}_{ij}=(x_j-x_i, y_j-y_i)$, and $|\vec{r}_{ij}|$ is the distance between the collocation point, j, and the Stokeslet, i. The Einstein summation rule applies to superscript m.

DOI: 10.1002/fld

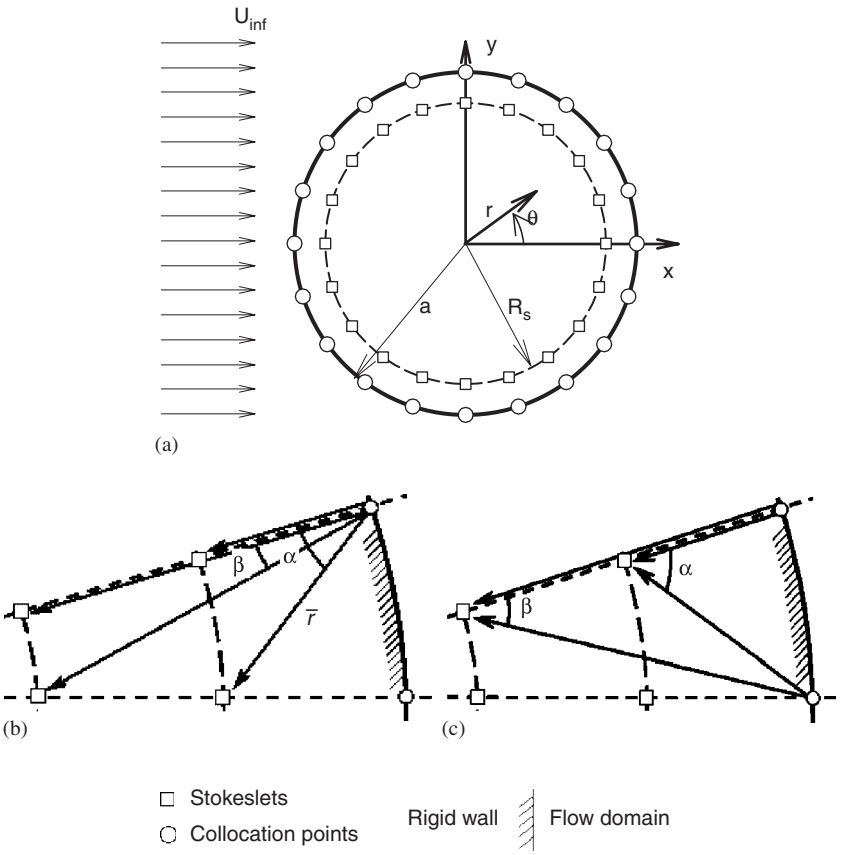

Figure 1. Schematic of the problem: (a) flow past an infinitely long cylinder with Stokeslets and collocation points shown; (b) vectors directed from a collocation point to two neighboring Stokeslets; and (c) vectors directed from two neighboring collocation points to a Stokeslet. Here, α and β are angles between vectors, where the angle β corresponds to a deeper submergence of Stokeslets.

Owing to the logarithmic term in Equations (2) and (3), the two-dimensional Stokeslet exhibits a singular behavior not only when the observation point tends to the location of the Stokeslet, but also when the observation point is far away from the location of the Stokeslet ($|\vec{r}| \to \infty$). The singularity at $|\vec{r}| \to \infty$ suggests that the solution is invalid far away from the location of the Stokeslet. Nevertheless, it does not cause numerical problems since the distance between the collocation point and the location of a Stokeslet is limited to finite values in the present computations. Three versions of the MFS, which remove the singularity at $|\vec{r}| = 0$, have been investigated for the three-dimensional flow about a single sphere [26]. It was shown in our recent study [26] that the application of the submerged Stokeslets generated satisfactory results for partial-slip flows without extra efforts to obtain the correct pressure at the fluid–solid interface. Hence, the submerged Stokeslets are used in this study.

DOI: 10.1002/fld

The pressure induced by a Stokeslet was presented in [25] as

$$p = -\frac{1}{2\pi}\frac{F^{(i)}r^{(i)}}{|\vec{r}|^2} \tag{4}$$

Thus, the pressure at point 'j' caused by N Stokeslets can be expressed as

$$p_j = -\frac{1}{2\pi}\sum_{i=1}^{N}\frac{F_i^{(m)}r_{ij}^{(m)}}{|\vec{r}_{ij}|^2} \tag{5}$$

The solution procedure by direct collocation is as follows. By substituting Equation (3) into BC (1), a system of linear equations was constructed. The strength of the Stokeslets, $\vec{F}$, was obtained by solving this system. The velocity vector in the domain of the fluid flow was then calculated straightforwardly by using Equation (3). In the formation of the linear system, the derivatives of velocity in BC (1) in the polar coordinates are obtained by differentiating Equation (3) for velocity at the rigid boundary (see Appendix A for details).

3. VALIDATION OF THE MFS

3.1. Flow past an infinitely long cylinder

A uniform flow past an infinite long cylinder was investigated first to verify the method of fundamental solutions of submerged Stokeslets. The cylinder with a radius a is located at the origin. The far-field flow velocity vector is $(1, 0)$ (see Figure 1(a)).

3.1.1. Analytical solution for flow past an infinitely long cylinder. Under the Stokes approximation, an analytical solution for a far-field uniform flow (U_{inf}) in the x direction past an infinitely long cylinder with its center at the origin was presented in [46] as

$$u = -\frac{1}{1-2\ln a}\left(-\left(2\ln r - \frac{a^2}{r^2}\right) + 2\frac{x^2}{r^2}\left(1-\frac{a^2}{r^2}\right)\right) + U_{\text{inf}} \tag{6a}$$

$$v = -\frac{2xy}{(1-2\ln a)r^2}\left(1-\frac{a^2}{r^2}\right) \tag{6b}$$

where $r = \sqrt{x^2+y^2}$. Because of the logarithmic term in Equation (6a) the solution is unbounded when $r \to \infty$ (the Stokes paradox). Nevertheless, this solution is valid in the area close to the cylinder [47]. This two-dimensional flow was used as a benchmark for the method of regularized Stokeslets in [46].

3.1.2. Accuracy of numerical results for no-slip flows. The streamlines are presented in Figure 2(b) for the no-slip flow past a cylinder. They coincide with the experimental streamlines for Stokes flow about a cylinder [48]. It can be observed from Figure 2(b) that the flow is reversible and symmetric about the line of $y = 0$, which is typical for uniform Stokes flows past a solid body.

DOI: 10.1002/fld

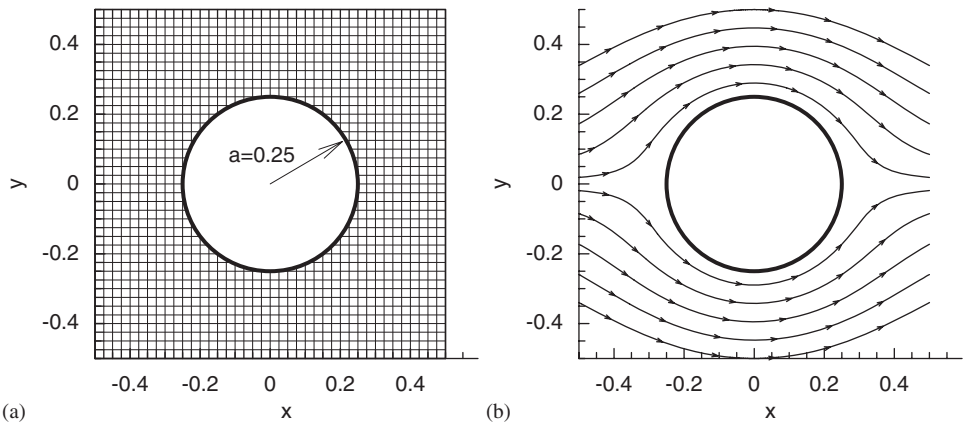

Figure 2. Computed flowfield for flow about an infinitely long cylinder: (a) the 41×41 grid for convergence evaluation in the $2a \times 2a$ domain and (b) streamlines for no-slip boundary conditions.

The accuracy of the numerical results of the Stokes flow about a cylinder is evaluated by comparing with the analytical solution at the 41×41 grid covering the $2a \times 2a$ domain enclosing the cylinder (see Figure 2(a)). It should be noted that this mesh is used exclusively for convergence evaluation. The solution procedure involves only the boundary discretization (see Figure 1). The formula used for calculating the error of velocity magnitude is

$$\mathrm{Err}_v = \frac{\sum_{j=1}^{N_y} \sum_{i=1}^{N_x} ||\mathbf{u}_{i,j}^{\mathrm{num}}| - |\mathbf{u}_{i,j}^{\mathrm{an}}||}{N} \tag{7}$$

where $N_x = N_y = 41$. The superscripts 'num' and 'an' denote the numerical and analytical results, respectively.

Presented in Figure 3 are the errors of velocity magnitude with respect to the submergence depth and the number of Stokeslets obtained by using Equation (7). For the fixed number of Stokeslets, the error of the numerical results decreases with the increase in the submergence depth. For example, if the number of Stokeslets is $N = 20$, the error in the velocity magnitude reaches $\mathrm{O}(10^{-10})$ when the submergence depth is 80% of the cylinder radius.

It can be observed in Figure 3 that the accuracy increases with the increase in the number of Stokeslets for a fixed submergence depth. The maximum accuracy achieved by varying the submergence depth decreases with the decrease in the number of Stokeslets employed. In order to achieve a prescribed accuracy, the deeper the Stokeslets are submerged, the smaller the number of Stokeslets required. However, the solution may fail if the submergence depth is too large. For example, for $N = 100$ the solution failed before the submergence depth reached the 90% of the cylinder radius. The reason for the failure could be attributed to the highly ill-conditioned matrix of the system, which has been reported in the literature [49, 50] and extensively addressed in our previous study for three-dimensional Stokeslets [26]. When the submergence depth of Stokeslets increases the system matrix become ill posed because of the following reasons: (i) the vectors directed from a collocation point to the neighboring Stokeslets become nearly parallel (see Figure 1(b)) and (ii) the vectors directed from neighboring collocation points to a Stokeslet

DOI: 10.1002/fld

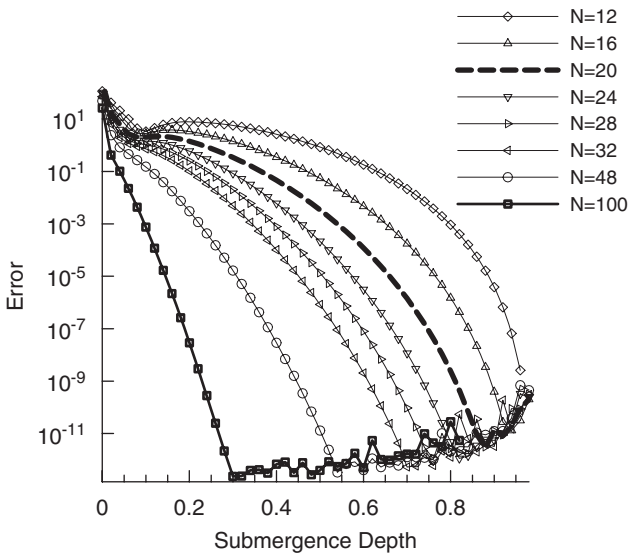

Figure 3. Errors of velocity magnitude with respect to the submergence depth and the number of Stokeslets used. The submergence depth is normalized by the radius of the cylinder.

become nearly parallel to each other (see Figure 1(c)). As a result, the system matrix contains almost equal columns or rows originated from the neighboring Stokeslets or collocation points.

It was stated in [43] that the numerical results obtained for the two-sphere problems by collocation schemes were sensitive to the distribution and the parity (even or odd) of the number of Stokeslets. Four cases are thus investigated to examine whether the sensitivity exist for the Stokes flow about the cylinder (see Figure 4). The number of Stokeslets is either 20 or 21. The Stokeslets are distributed evenly with the step $\Delta\theta$ with the first Stokeslet located either at $\theta=0$ or $\theta=\frac{1}{2}\Delta\theta$. The errors in the numerical results are presented in Figure 4 with respect to the submergence depth that ranges from 0 to 100% of the cylinder radius. No obvious advantage is observed of one case over the other.

3.1.3. Numerical independence of results on the submergence of Stokeslets for partial-slip and no-slip flows. As shown in the previous subsection for no-slip flows, the error of the numerical results decreases with the increase in the submergence depth. The independence of numerical results on the location of Stokeslets is evaluated for no-slip and partial-slip flows past an infinite long cylinder by using the following formula:

$$\mathrm{Err}_v = \frac{\mathrm{Max}_{i=1,N_s,j=1,N_y}(||\mathbf{u}_{i,j}^{n+1}|-|\mathbf{u}_{i,j}^{n}||)}{\mathrm{Max}_{i=1,N_s,j=1,N_y}(|\mathbf{u}_{i,j}^{n}|)} \tag{8}$$

where '$n+1$' and 'n' denote different submergence depths. The submergence depth ranges from 1 to 0.02 with a step of 0.02. The grid used for calculating the error is the same as that used in the previous section.

DOI: 10.1002/fld

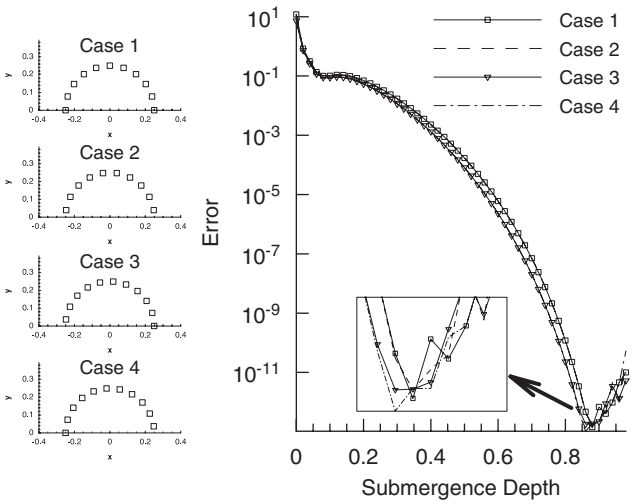

Figure 4. Error of velocity magnitude with respect to the submergence depth for different arrangement of Stokeslets: for Case 1 and Case 2, $N=20$; for Case 3 and Case 4, $N=21$; the starting point for discretization along the cylinder for Case 1 and Case 3 is at $\theta=0$ and that for Case 2 and Case 4 is at $\theta=\frac{1}{2}\Delta\theta$.

The number of Stokeslets used in the computations is equal to 20 based on the findings for the no-slip flows. Figure 5 shows the errors of velocity magnitude for no-slip ($Kn=0$) BC by using Equations (7) and (8) and partial-slip ($Kn=0.1$) BC by using Equation (8). It is observed that the error is small when the submergence depth is substantial. Note that the profiles of errors in velocity magnitude as a function of submerging depth are similar by using Equations (7) and (8).

3.2. Taylor–Couette flow

The flow confined in the gap between two concentric rotating cylinders is studied numerically to illustrate the applicability of the proposed methodology to partial-slip interior flows. The inner cylinder moves clockwise at the tangential velocity of U_i and the outer cylinder moves counter-clockwise at the tangential velocity of U_o (see Figure 6(a)). The center of the two concentric cylinders is located at the origin.

3.2.1. Analytical solution for the Taylor–Couette flow. The tangential velocity of the flow can be written in terms of the radius r in the polar coordinates as

$$u_\theta = C_1 r + \frac{C_2}{r}$$

where

$$C_1 = \frac{ab(U_\mathrm{o}b - U_\mathrm{i}a) + 2c(U_\mathrm{i}a^2 + U_\mathrm{o}b^2)}{ab(b^2-a^2) + 2c(b^3+a^3)}$$

$$C_2 = -\frac{a^2b^2(U_\mathrm{i}b - U_\mathrm{o}a)}{ab(b^2-a^2) + 2c(b^3+a^3)}$$

DOI: 10.1002/fld

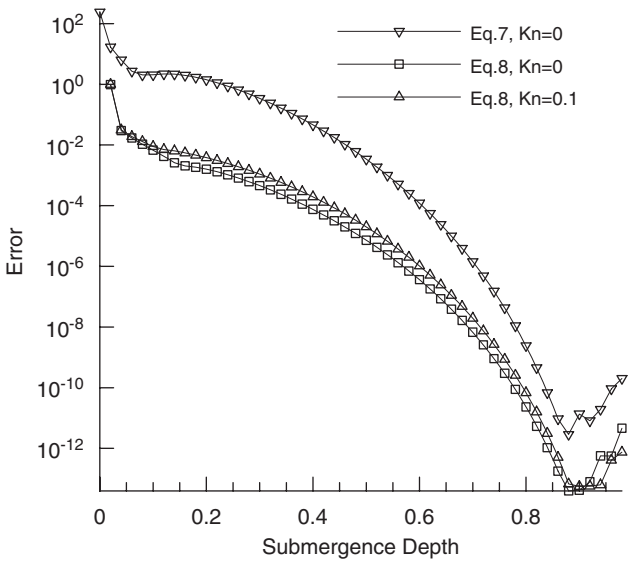

Figure 5. Error of velocity magnitude with respect to the submergence depth for the no-slip and partial-slip ($Kn=0.1$) flows about an infinitely long cylinder. Two different error norms (Equations (7) and (8)) are used.

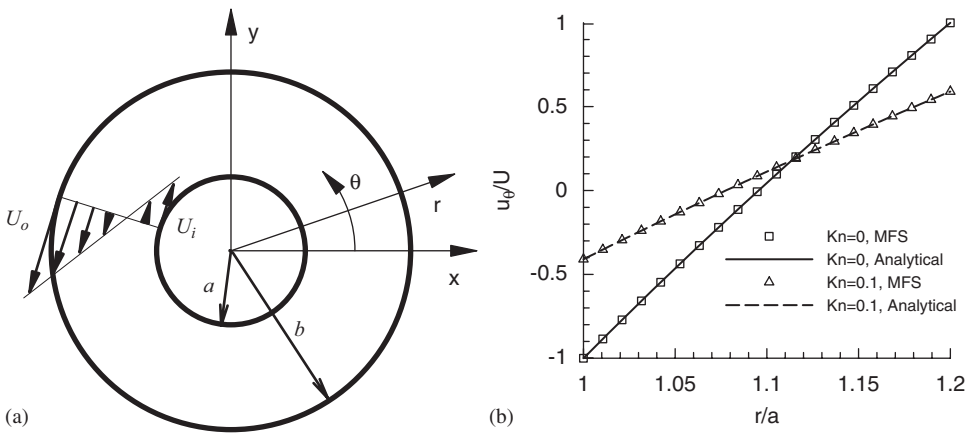

Figure 6. Taylor–Couette flow: (a) problem schematic and (b) the tangential velocity with respect to the radius r in the gap between two cylinders.

where a is the radius of the inner cylinder, b is the radius of the outer cylinder, c is the slip coefficient as described in Section 2. When c equals zero for no-slip flows, the coefficients C_1 and C_2 reduce to the ones presented in [47].

DOI: 10.1002/fld

3.2.2. Comparison of numerical results with the analytical solution. In the presented computations, the inner and outer cylinders rotate at a speed of U in the opposite directions. The radii of the inner and outer cylinder are 1 and 1.2, respectively. The number of Stokeslets used for the inner cylinder is 20 and the submergence depth for the Stokeslets is $0.8a$, as obtained from the previous computation for flow past a cylinder. The number of Stokeslets for the outer cylinder is 24 so that the distance between the neighboring collocation points is the same as that for the inner cylinder. The optimal submergence depth of Stokeslets for the outer cylinder is obtained in the same manner as adopted in Section 3.1.

The tangential velocity at $\theta=0$ is presented in Figure 6(b) along the r direction. The Knudsen number is based on the radius of the inner cylinder. A good agreement between the analytical and numerical results is observed for both no- and partial-slip BC. When the Knudsen number increases from 0 (no slip) to 0.1 (partial slip), the momentum transfer from the boundary to the fluid confined in the gap of the two cylinders is lowered substantially. At the surface of the inner cylinder, the tangential fluid velocity is less than the half of the wall velocity. At the surface of the outer cylinder, the tangential fluid velocity slightly exceeds the half of the wall velocity.

4. APPLICATIONS TO FILTRATION FLOW: PRESSURE DROP ACROSS A FILTER AND VELOCITY DISTRIBUTION FOR NO-SLIP AND PARTIAL-SLIP FILTRATION FLOWS

4.1. Problem setup

The schematic of the problem is given in Figure 7. The BC adopted for the numerical modeling are as follows. At the fiber surface, the BC determined by Equation (1) are applied. At the inlet, the velocity vector is $(0,-1)$. No BC are enforced at the outlet. At the planar walls, the partial-slip and no-penetrating BC are applied. In the computations, $\alpha=\beta=6, \gamma=\alpha/2$ (see Figure 7).

A representative set of 4×8 cylinders is taken to investigate the effects of the submergence depth of Stokeslets and the side wall length on the computed pressure drop.

The pressure drop presented is an average one across a row of fibers and calculated as $\Delta p=(\bar{p}_2-\bar{p}_1)/(N_r-2)$, where N_r is the number of rows of fibers, $\bar{p}_1$ and $\bar{p}_2$ are the average pressures at two horizontal cross-sections, y_1 and y_2, and subscript 'num' denotes the numerical result, $y=y_1$ is the cross-section in the middle of the bottom row of cylinders and its neighboring row and $y=y_2$ is one in the middle of the top row of cylinders and its neighboring row. The distributions of collocation points and locations of Stokeslets are shown in Figure 8.

In Figure 9, it is shown that the pressure drop tends to a constant value when the submergence depth of Stokeslets and the wall length increase, which validates the independence of the numerical results over the setup length and the submergence depth of Stokeslets.

4.2. Comparison with experiments

In the experimental study [45], no-slip filtration flows were investigated with respect to the velocity distributions and pressure drop across a filter. The Reynolds number of the filtration flow under investigation ranged from 0.01 to 0.17. The distances of separation between the centers of rods were equal in the vertical and horizontal directions and denoted by a single symbol, D. The corresponding setup in the numerical computation is $\alpha=\beta=D/a$. The experimental results of velocity and pressure drop for the case of packing function $c_{pf}=5\%$ are compared with the results

DOI: 10.1002/fld

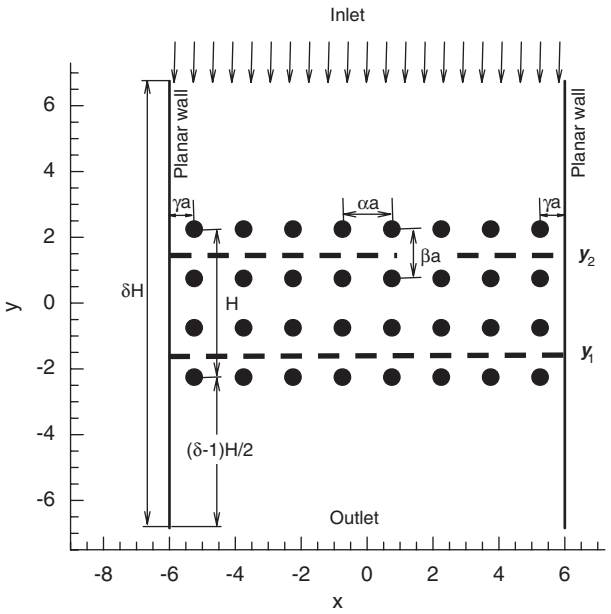

Figure 7. Setup for the flow about a representative 4×8 set of cylindrical fibers. The distances between neighboring columns and rows are denoted as αa and βa, respectively (where a is the radius of fiber), the distance between the centers of fibers at the outmost layer of cylinders in the x direction and the adjacent wall is denoted as γa. The height of the filtering layer (i.e. the distance between the centers of two outmost rows of cylinders) is denoted as H. A similar geometry setup was used in the experimental research.

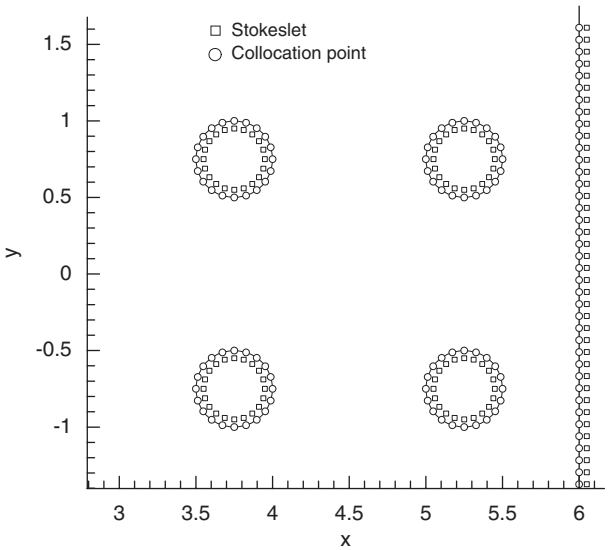

Figure 8. Distribution of collocation points and Stokeslets for flow about multiple fibers.

DOI: 10.1002/fld

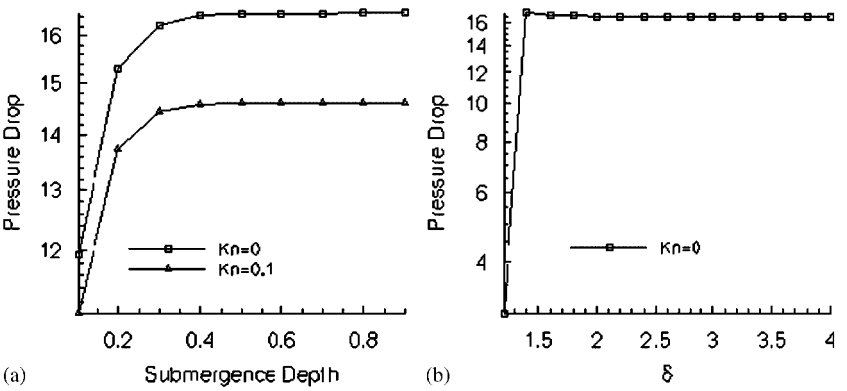

Figure 9. Obtained pressure drop: (a) pressure drop with respect to the submergence depth of Stokeslets and (b) pressure drop with respect to the wall length, δH.

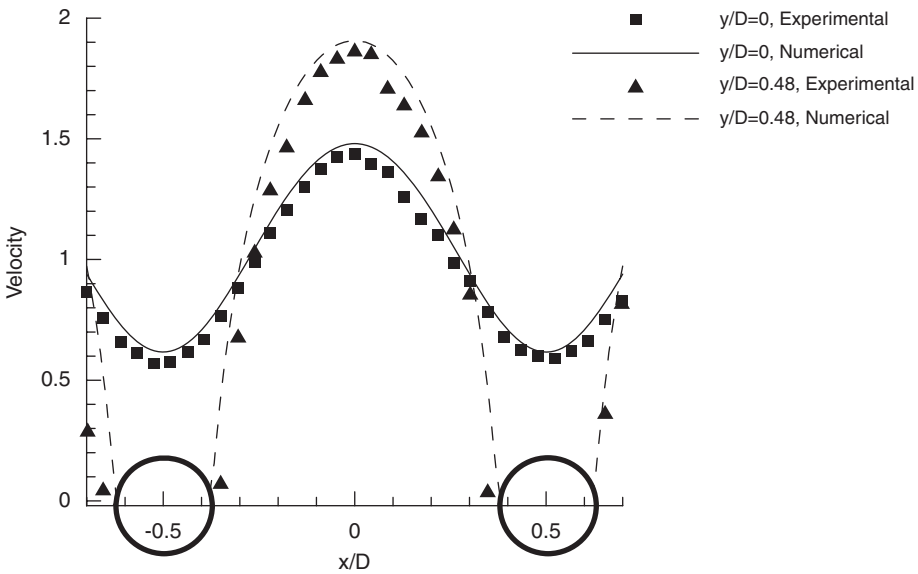

Figure 10. Comparison between numerical and experimental results: velocity profiles along two horizontal cross-sections at $y/D=0$ and $y/D=0.48$. Here, D is the distance of separation of the centers of fibers.

from numerical modeling. Here, c_{pf} is defined as $c_{\mathrm{pf}}=\pi a^2/D^2$ that corresponds to $\alpha=\beta=\sqrt{\pi/c_{\mathrm{pf}}}=7.93$. The number of rows of rods is 8 and the number of columns is 14. It is shown in Figure 10 that the numerical velocity profiles agree well with the experimental results. The difference in the pressure drop is $(\Delta p_{\mathrm{num}}-\Delta p_{\mathrm{exp}})/\Delta p_{\mathrm{exp}}\approx -6.7\%$, where subscript 'exp' denotes the experimental result. The fact that the numerical pressure drop is less than the experimental one can be attributed to the two-dimensional assumption made in the numerical modeling.

DOI: 10.1002/fld

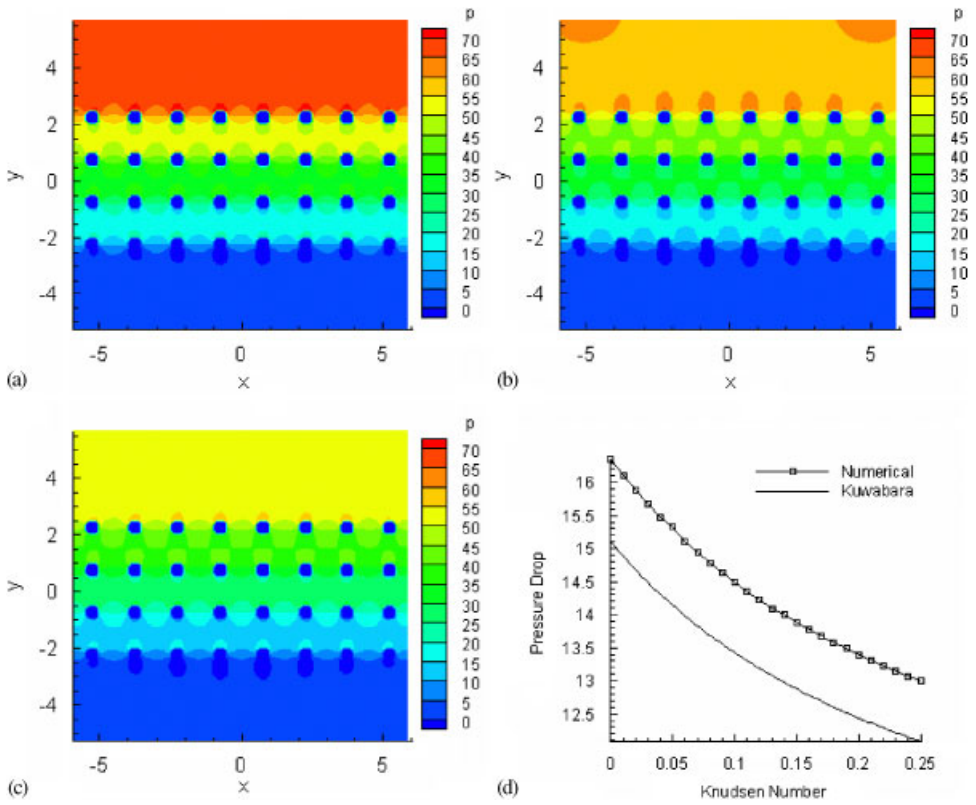

Figure 11. Pressure with respect to the Knudsen number: (a) pressure distributions for $Kn=0$ (no slip); (b) $Kn=0.1$ (partial slip); (c) $Kn=0.25$ (partial slip); and (d) comparison of pressure drop between numerical and analytical results by Kuwabara model.

4.3. Comparison with Kuwabara's model

In Kuwabara's model, a two-dimensional velocity field of viscous flow transverse to a cylinder with symmetrical BC was used to model the filtration flow through a parallel set of cylindrical fibers. The formula of pressure drop based on Kuwabara's model was presented in [1]

$$\Delta p = \frac{4\mu c_{\mathrm{pf}} h U_{\mathrm{inf}} (1+1.996Kn)}{a^2\left[-\frac{1}{2}\ln(c_{\mathrm{pf}}) - 0.75 + c_{\mathrm{pf}} - \frac{c_{\mathrm{pf}}^2}{4} + 1.996Kn\left(-\frac{1}{2}\ln(c_{\mathrm{pf}}) - 0.25 + \frac{c_{\mathrm{pf}}^2}{4}\right)\right]} \tag{9}$$

where μ is the viscosity, h is the thickness of filter, U_{inf} is the far-field velocity and a is the radius of fiber. The upper limit of the Knudsen number for Kuwabara's model to remain valid is 0.25.

It should be noted that the assumption used for deriving the analytical solution presented in Equation (9) is the infinite number of cylinders in the y direction. Despite of this discrepancy between the numerical and analytical setups, the analytical formula was still valuable for

DOI: 10.1002/fld

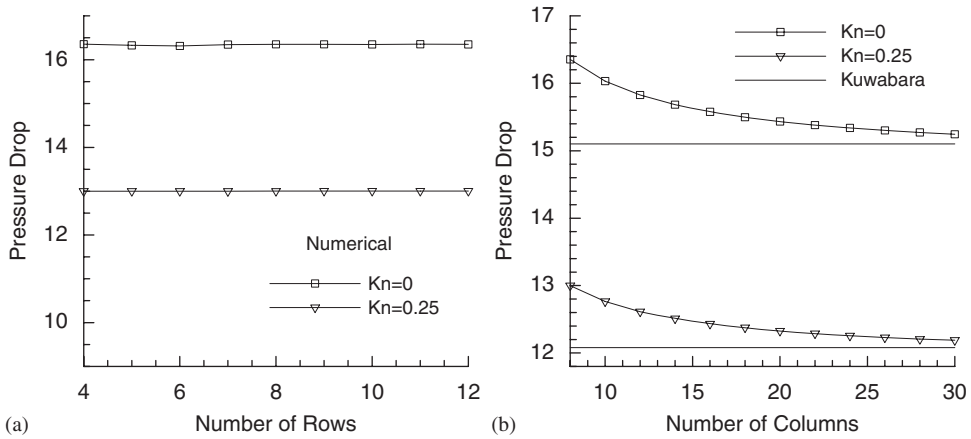

Figure 12. Pressure drop with respect to: (a) number of rows and (b) number of columns.

approximately examining the validity of the numerical simulation and investigating the wall effects on pressure drop.

By using the same geometry setup as described in Section 4.1, the pressure contours for no-slip and partial-slip filtration flows ($Kn = 0.1$ and 0.25) are obtained and presented in Figure 11(a)–(c), respectively. The pressure distribution roughly exhibits stratification in the y direction corresponding to hydraulic losses of flow energy. It is observed that the pressure for the no-slip case in the entrance area is much higher than those for the partial-slip cases for the same pressure in the exit area. Thus, the partial-slip at the fluid–solid interface lowers the pressure drop. In Figure 11(d), the pressure drop is given as a function of the Knudsen number. With the increase of the Knudsen number, the numerical and analytical pressure drops follow a similar tendency. The discrepancy between the numerical and analytical pressure drops exists because of the presence of planar walls and the finite number of fibers in the numerical computations.

Further computations are conducted to investigate the influence of the number of columns and rows of cylinders on the pressure drop. It is observed that the increase in number of rows barely affects the pressure drop (see Figure 12(a)). The numerical pressure drop evolves rapidly and tends to the value calculated from the Kuwabara model (Equation (9)) when the number of fibers' columns increases (see Figure 12(b)).

5. CONCLUSIONS

In this study the MFS for two-dimensional partial-slip flows is developed and validated. The accuracy of the numerical results is examined in terms of the number of Stokeslets and the submergence depth of Stokeslets. It is shown that a prescribed accuracy of the numerical results can be maintained using the largely reduced number of Stokeslets if the optimal submergence depth of Stokeslets is chosen. The reduction in the number of Stokeslets used per fiber leads to the reduction in the size of the formed matrix, and thus the computational cost is greatly reduced.

DOI: 10.1002/fld

The sensitivity of the numerical solution to the parity of the number of Stokeslets and to the distribution of Stokeslets is investigated.

The developed approach is then applied to the representative sets of cylinders confined between two planar walls typical for filtration flows. The numerical results agree very well with the experimental results for no-slip filtration flows. The numerical results for no-slip and partial-slip flows are compared with Kuwabara's model, which represent a limit case with infinitely large number of columns and rows of fibers. It is demonstrated that the slip at fluid–solid interfaces has a significant effect over the pressure drop. This effect is adequately captured by the proposed method of fundamental solutions for partial-slip flows.

The current study will be extended to filtration flows in the transition flow regime in the near future. For transition flows, heuristic slip models are not sufficient to account for the effect of the near-wall Knudsen layer. The direct simulation Monte Carlo for the Knudsen layer will be combined with the MFS methodology developed in the current study.

APPENDIX A

The Cartesian velocity components in Equation (2) can be explicitly expressed as

$$\begin{aligned} u_x = u_j^{(1)} &= \frac{1}{4\pi\mu}\left(F_i^{(1)} \ln|\vec{r}_{ij}| - \frac{F_i^{(1)} r_{ij}^{(1)} + F_i^{(2)} r_{ij}^{(2)}}{|\vec{r}_{ij}|^2} r_{ij}^{(1)}\right) \\ u_y = u_j^{(2)} &= \frac{1}{4\pi\mu}\left(F_i^{(2)} \ln|\vec{r}_{ij}| - \frac{F_i^{(1)} r_{ij}^{(1)} + F_i^{(2)} r_{ij}^{(2)}}{|\vec{r}_{ij}|^2} r_{ij}^{(2)}\right) \end{aligned} \tag{A1}$$

Indices 'i' and 'j' are omitted for brevity in the following development.

The relation between the Cartesian and polar coordinates (r, θ) is given as follows:

$$(x, y) = (r\cos\theta, r\sin\theta)$$

The velocity in the polar coordinates, $\mathbf{u}_\mathrm{p}$, can be related to the velocity in the Cartesian coordinates, $\mathbf{u}_\mathrm{c}$, as follows:

$$\mathbf{u}_\mathrm{p} = M\,\mathbf{u}_\mathrm{c} \tag{A2}$$

where

$$\mathbf{u}_\mathrm{p} = \begin{bmatrix} u_r \\ u_\theta \end{bmatrix}, \quad \mathbf{u}_\mathrm{c} = \begin{bmatrix} u_x \\ u_y \end{bmatrix}, \quad M = \begin{bmatrix} n_x & n_y \\ \theta_x & \theta_y \end{bmatrix}$$

(n_x, n_y) and (θ_x, θ_y) are unit vectors in the r and θ directions.

Using the above relations and the formulas (A1), one can obtain

$$\begin{aligned} u_\theta &= \frac{1}{4\pi\mu}\,\vec{\theta}\cdot R\cdot\vec{F} \\ u_r &= \frac{1}{4\pi\mu}\,\vec{n}\cdot R\cdot\vec{F} \end{aligned} \tag{A3}$$

DOI: 10.1002/fld

$$\frac{\partial u_r}{\partial \theta} = \frac{1}{4\pi\mu}(n_x \vec{\theta}' \cdot A \cdot \vec{F} + n_y \vec{\theta}' \cdot B \cdot \vec{F} + \vec{\theta}'' \cdot R \cdot \vec{F})$$

$$\frac{\partial u_\theta}{\partial r} = \frac{1}{4\pi\mu}(\theta_x \vec{n} \cdot A \cdot \vec{F} + \theta_y \vec{n} \cdot B \cdot \vec{F})$$

where

$$\mathbf{F} = (F^{(1)}, F^{(2)})^{\mathrm{T}}$$

$$\mathbf{n} = (n_x, n_y) = (\cos\theta, \sin\theta)$$

$$\boldsymbol{\theta} = (\theta_x, \theta_y) = (-\sin\theta, \cos\theta)$$

$$\vec{\theta}' = \left(\frac{\partial x}{\partial \theta}, \frac{\partial y}{\partial \theta}\right) = (-r\sin\theta, r\cos\theta)$$

$$\vec{\theta}'' = \left(\frac{\partial n_x}{\partial \theta}, \frac{\partial n_y}{\partial \theta}\right) = (-\sin\theta, \cos\theta)$$

$$R = \begin{bmatrix} \left(-\dfrac{r^{(1)}r^{(1)}}{|\vec{r}|^2} + \ln|\vec{r}|\right) & \left(-\dfrac{r^{(1)}r^{(2)}}{|\vec{r}|^2}\right) \\ \left(-\dfrac{r^{(2)}r^{(1)}}{|\vec{r}|^2}\right) & \left(-\dfrac{r^{(2)}r^{(2)}}{|\vec{r}|^2} + \ln|\vec{r}|\right) \end{bmatrix}$$

$$A = \begin{bmatrix} \left(-\dfrac{r^{(1)}}{|\vec{r}|^2} + 2\dfrac{r^{(1)}r^{(1)}r^{(1)}}{|\vec{r}|^4}\right) & \left(-\dfrac{r^{(2)}}{|\vec{r}|^2} + 2\dfrac{r^{(1)}r^{(1)}r^{(2)}}{|\vec{r}|^4}\right) \\ \left(\dfrac{r^{(2)}}{|\vec{r}|^2} + 2\dfrac{r^{(1)}r^{(1)}r^{(2)}}{|\vec{r}|^4}\right) & \left(-\dfrac{r^{(1)}}{|\vec{r}|^2} + 2\dfrac{r^{(1)}r^{(2)}r^{(2)}}{|\vec{r}|^4}\right) \end{bmatrix}$$

$$B = \begin{bmatrix} \left(-\dfrac{r^{(2)}}{|\vec{r}|^2} + 2\dfrac{r^{(1)}r^{(1)}r^{(2)}}{|\vec{r}|^4}\right) & \left(\dfrac{r^{(1)}}{|\vec{r}|^2} + 2\dfrac{r^{(1)}r^{(2)}r^{(2)}}{|\vec{r}|^4}\right) \\ \left(-\dfrac{r^{(1)}}{|\vec{r}|^2} + 2\dfrac{r^{(1)}r^{(2)}r^{(2)}}{|\vec{r}|^4}\right) & \left(-\dfrac{r^{(2)}}{|\vec{r}|^2} + 2\dfrac{r^{(2)}r^{(2)}r^{(2)}}{|\vec{r}|^4}\right) \end{bmatrix}$$

It should be noted that the above formulas are presented for a single Stokeslet. For N Stokeslets, the right-hand side of (A3) should be summarized over the number of Stokeslets. Replacing the

DOI: 10.1002/fld

corresponding terms in partial-slip BC (1), two equations at a collocation point can be obtained as,

$$\sum\left(\left(\vec{\theta}\cdot R - c\left(\frac{1}{r}(n_x\vec{\theta}'\cdot A + n_y\vec{\theta}'\cdot\vec{\theta}''\cdot R)\right.\right.\right.$$
$$\left.\left.\left.-\frac{1}{r}(\vec{\theta}\cdot R + \theta_x\vec{n}\cdot A + \theta_y\vec{n}\cdot B)\right)_{r=a}\right)\cdot\vec{F}\right) = 4\pi\mu u_{s\theta} \tag{A4}$$
$$\sum(\vec{n}\cdot R\cdot\vec{F}) = 4\pi\mu u_{sr}$$

When $c=0$, the first equation reduces to

$$\sum(\vec{\theta}\cdot R\cdot\vec{F}) = 4\pi\mu u_{s\theta}$$

that corresponds to the no-slip BC.

For N collocation points, one can obtain $2N$ equations (A4) with respect to N unknown Stokeslets **F**. It should be noted that matrices A and B originate from the derivatives of velocity, and hence involve derivatives of Stokeslets, that is, higher-order singularities.

REFERENCES

1. Brown RC. *Air Filtration*: *An Integrated Approach to the Theory and Applications of Fibrous Filters*. Pergamon Press: New York, 1993.
2. Dhaniyala S, Liu BYH. Investigations of particle penetration in fibrous filters: part I experimental. *Journal of the IEST* 1999; **42**(1):32–40.
3. Dhaniyala S, Liu BYH. Investigations of particle penetration in fibrous filters: part II theoretical. *Journal of the IEST* 1999; **42**(2):40–46.
4. Kuwabara S. The forces experienced by randomly distributed parallel circular cylinders or spheres in a viscous flow at small Reynolds numbers. *Journal of Physical Society of Japan* 1959; **14**:527–532.
5. Happel J. Viscous flow relative to arrays of cylinders. *AIChE Journal* 1959; **5**:174–177.
6. Lee KW, Liu BYH. Theoretical study of aerosol filtration by fibrous filters. *Aerosol Science and Technology* 1982; **1**:147–161.
7. Zhu C, Lin CH, Cheung CS. Inertial impaction-dominated fibrous filtration with rectangular or cylindrical fibers. *Powder Technology* 2000; **112**:149–162.
8. Dunnett SJ, Clement CF. A numerical study of the effects of loading from diffusive deposition on the efficiency of fibrous filters. *Journal of Aerosol Science* 2006; **37**:1116–1139.
9. Ouyang M, Liu BYH. Analytical solution of flow field and pressure drop for filters with rectangular fibers. *Journal of Aerosol Science* 1998; **29**:187–196.
10. Fuchsa NA, Kirsch AA, Stechkina IB. A contribution to the theory of fibrous aerosol filters. *Faraday Symposia of the Chemical Society* 1973; **7**:143–156.
11. Karniadakis GE, Beskok A. *Micro Flows*: *Fundamentals and Simulation*. Springer: New York, 2002.
12. Rubow KL. Submicron aerosol filtration characteristics of membrane filters. *Ph.D. Dissertation*, Mechanical Engineering Department, University of Minnesota, Minneapolis, MN, 1981.
13. Kanaoka C, Hiragi S, Tanthapanichakoon W. Stochastic simulation of the agglomerative deposition process of aerosol particles on an electret fiber. *Powder Technology* 2001; **118**:97–106.
14. Shin C. Filtration application from recycled expanded polystyrene. *Journal of Colloid and Interface Science* 2006; **302**(1):267–271.
15. Polyakov Y. Particle deposition in outside-in hollow fiber filters and its effect on their performance. *Journal of Membrane Science* 2006; **278**(1–2):190–198.
16. Ramakrishna S *et al.* Polymer nanofibers for biosensor applications. *Molecular Building Blocks for Nanotechnology*: *From Diamondoids to Nanoscale Materials and Applications*, Chapter 16. Springer: New York, 2007; 377–392.

DOI: 10.1002/fld

17. Lauga E, Squires TM. Brownian motion near a partial-slip boundary: a local probe of the no-slip condition. *Physics of Fluids* 2005; **17**:103102-1–103102-16.
18. Bonaccurso E, Kappl M, Butt H-J. Hydrodynamic force measurements: boundary slip of water on hydrophilic surfaces and electro kinetic effects. *Physics Review Letters* 2002; **88**(8):076103-1–176103-4.
19. Zhu YX, Granick S. Rate-dependent slip of Newtonian liquid at smooth surfaces. *Physics Review Letters* 2001; **87**(9):096105-1–096105-3.
20. Alves CJS, Silvestre AL. Density results using Stokesltes and a method of fundamental solutions for the Stokes equations. *Engineering Analysis with Boundary Elements* 2004; **28**:1245–1252.
21. Young DL, Jane SJ, Fan CM, Murugesan K, Tsai CC. The method of fundamental solutions for 2D and 3D Stokes flows. *Journal of Computational Physics* 2006; **211**:1–8.
22. Karadimos A, Ocone R. The effect of the flow field recalculation on fibrous filter loading: a numerical simulation. *Powder Technology* 2003; **137**:109–119.
23. Liu ZG, Wang PK. Numerical investigation of viscous flow fields around multifiber filters. *Aerosol Science and Technology* 1996; **25**:375–391.
24. Kirsch VA. Stokes flow in model fibrous filters. *Separation and Purification Technology* 2007; **58**:288–294.
25. Pozrikidis C. *Boundary Integral and Singularity Methods for Linearized Viscous Flow*. Cambridge University Press: New York, 1992.
26. Zhao S, Povitsky A. Boundary singularity method for partial-slip flows. Presented at the *37th AIAA Fluid Dynamics Conference and Exhibition*, Miami, FL, June 2007. *AIAA Paper 2007-3989*.
27. Zhao S, Povitsky A. Method of submerged Stokeslets for slip flow about ensembles of particles. *Journal of Nanoscience and Nanotechnology* 2008; **8**(8):3790–3801.
28. Young DL, Chen CW, Fan CM, Murugesan K, Tsai CC. The method of fundamental solutions for Stokes flow in a rectangular cavity with cylinders. *European Journal of Mechanics B/Fluids* 2005; **24**:703–716.
29. Zhou H, Pozrikidis C. Adaptive singularity method for Stokes flow past particles. *Journal of Computational Physics* 1995; **117**:79–89.
30. Götz T. Simulating particles in Stokes flow. *Journal of Computational and Applied Mathematics* 2005; **175**: 415–427.
31. Tsai CC, Young DL, Lo DC, Wong TK. Method of fundamental solutions for three-dimensional Stokes flow in exterior field. *Journal of Engineering Mechanics* 2006; **132**:317–326.
32. Lighthill J. Helical distributions of stokeslets. *Journal of Engineering Mathematics* 1996; **30**:35–78.
33. Cortez R, Fauci L, Medovikov A. The method of regularized Stokeslets in three dimensions: analysis, validation, and application to helical swimming. *Physics of Fluids* 2005; **17**:031504-1–031504-14.
34. Wang W, Parker KH. Movement of spherical particles in capillaries using a boundary singularity method. *Journal of Biomechanics* 1998; **31**:347–354.
35. Shu JJ, Chwang AT. Generalized fundamental solutions for unsteady viscous flows. *Physical Review E* 2001; **63**:051201-1–051201-7.
36. Tsai CC, Young DL, Fan CM, Chen CW. MFS with time-dependent fundamental solutions for unsteady Stokes equations. *Engineering Analysis with Boundary Elements* 2006; **30**(10):897–908.
37. Chen CW, Young DL, Tsai CC, Murugesan K. The method of fundamental solutions for inverse 2D Stokes problems. *Computational Mechanics* 2005; **37**:2–14.
38. Tsai CC. Solutions of slow Brinkman flows using the method of fundamental solutions. *International Journal of Numerical Methods in Fluids* 2008; **56**:927–940.
39. Mathon R, Johnston RL. The approximate solution of elliptic boundary-value problems by fundamental solutions. *SIAM Journal on Numerical Analysis* 1977; **14**(4):638–650.
40. Fairweather G, Karageorghis A. The method of fundamental solutions for elliptic boundary value problems. *Advances in Computational Mathematics* 1998; **9**:69–95.
41. Nishida K. Numerical method for Oseen's linearized equations in three-dimensional exterior domains. *Journal of Computational and Applied Mathematics* 2003; **152**:405–409.
42. Ogata H. A fundamental solution method for three-dimensional Stokes flow problems with obstacles in a planar periodic array. *Journal of Computational and Applied Mathematics* 2006; **189**:622–634.
43. Kim S, Karria SJ. *Microhydrodynamics*: *Principles and Selected Applications*. Butterworth-Heinemann: Boston, 1991.
44. Chwang AT, Yao-Tsu Wu T. Hydromechanics of low-Reynolds-number flow, part 2, singularity method for Stokes flows. *Journal of Fluid Mechanics* 1975; **67**(4):787–815.
45. Zhong WH, Currie IG, James DF. Creeping flow through a model fibrous porous media. *Experiments in Fluids* 2006; **40**:119–126.

DOI: 10.1002/fld

46. Cortez R. The method of regularized Stokeslets. *SIAM Journal on Scientific Computing* 2001; **23**(3):1204–1225.
47. Panton RL. *Incompressible Flow*. Wiley: New York, 1984.
48. Van Dyke M. *An Album of Fluid Motion*. The Parabolic Press: Stanford, CA, 1982.
49. Smyrlis YS, Karageorghis A. Some aspects of the method of fundamental solutions for certain harmonic problems. *Journal of Scientific Computing* 2001; **16**(3):341–371.
50. Balakrishnan K, Ramachandran PA. The method of fundamental solutions for linear diffusion-reaction equations. *Mathematical and Computer Modeling* 2000; **31**:221–237.

DOI: 10.1002/fld